Search templates for gravitational waves from precessing, inspiraling binaries

Theocharis A. Apostolatos*
Theoretical Astrophysics, California Institute of Technology, Pasadena, California 91125
(Received 6 March 1995)

Searches for gravitational waves with the LIGO-VIRGO-GEO detector network will require families of "search templates" with which to cross correlate the noisy detectors' output. This paper introduces a *fitting factor* (FF), as a quantitative measure of how well the best template in a family "fits" a hypothetical gravitational waveform, in the presence of a specific detector noise spectrum. An FF$<$ 0.9 corresponds to a 27% reduction in the event rate of the relevant signals; therefore a family of templates that leads to FF's below 0.9 should be considered inadequate. The FF is used to explore the adequateness of several families as search templates for gravitational waves from compact inspiraling binaries. The binaries are taken to move in circular orbits, and the "advanced LIGO noise spectrum" is assumed for the detectors. We first study the acceptability of the simplest three-parameter template family, the so-called "Newtonian family." From previous studies by Finn, Królak, Kokotas, Schäfer, Dhurandar, and Balasubramanian, we infer that post-Newtonian effects in the true waveforms of binaries with vanishing spins cause the Newtonian family to have an unacceptable low FF ($\sim$ 0.6 to 0.8). We then study the influence of waveform modulations caused by spin-induced orbital precession, and we isolate the modulation effects from other post-Newtonian effects by pretending that the true signals are pure Newtonian with modulation. Many different parameters influence the precession and then the waveform modulation. A wide range of parameter values is explored, and intuition is developed into which parameters most strongly influence the FF. It is shown that the unmodulated Newtonian template family works quite well (FF$>$ 0.9 for almost all parameter values) in searches for the modulated Newtonian signal from two $1.4M_\odot$ neutron stars (NS's) with one of them maximally spinning. By contrast, for a maximally spinning $10M_\odot$ black hole (BH) with a nonrotating $1.4M_\odot$ NS, the Newtonian template family produces FF$<$ 0.9 for more than half of all the binaries' orientations, if the spin and orbital angular momenta are misaligned by 30°. We introduce a new four-parameter template family, which has the form of the nonmodulated post^1-Newtonian signal from a zero-spin-binary. Although, there is a substantial improvement of the FF's for a spin-modulated Newtonian signal, the FF's for nonmodulated post$^{1.5}$-Newtonian waveforms are still very poor ($\sim$ 0.5–0.8). Therefore we propose another four-parameter template family that has the same form as a nonmodulated post$^{1.5}$-Newtonian signal with all the spin-related parameters stripped off. This template family works post$^{1.5}$-Newtonian modulated signals quite well. These results suggest that, in a few years, when waveforms have been computed up to post^3-Newtonian order, a good template family will be the four-parameter post^3-Newtonian waveforms for zero-spin binaries, augmented by some appropriate modulations to deal with misaligned, rapidly spinning BH-NS systems. Finally, we extend our investigations to the space-based low-frequency LISA detector.

PACS number(s): 04.80.Nn, 04.30.−w, 97.60.Jd, 97.60.Lf

I. INTRODUCTION

The facilities to house the ground-based LIGO-VIRGO laser-interferometer gravitational-wave detectors are already under construction or in the final stage of their design [1], and the GEO600 project for an intermediate scale interferometer has good prospects for approval. At about the turn of the century LIGO-VIRGO-GEO will probably be ready to start searching for gravitational waves coming from the most promising sources: neutron-star–neutron-star (NS-NS), neutron-star–black-hole (NS-BH), or black-hole–black-hole (BH-BH) binaries.

The detectability of these binaries depends on the family of "search templates" that will be used as matched filters to extract a possible signal buried in the detectors' noise. (For the method of "matched filters" see Ref. [2].) More specifically, the output data stream of each detector will be cross correlated with each template $T_{\lambda_1,\lambda_2,\ldots}$ of the chosen family, weighted by the inverse of the detector's noise spectrum. If for some combination of the templates' parameters $\lambda_1, \lambda_2, \ldots$ the cross-correlation output is above some threshold level, then a signal will have been detected with great confidence. Therefore, we should make sure that some member of the family of templates used for detection matches very well each of the hypothetical incoming waveforms.

The true general relativistic signals from inspiraling binaries (including post-Newtonian and spin-induced effects) depend on a very large set of parameters (the masses of the two stars, the eccentricity of their orbit,

*Present address: M.P.G. Arbeitsgruppe Gravitationstheorie, Friedrich Shiller Universität Jena, Max-Wien-Platz 1, D 07743, Jena, Germany.

their spin, the relative geometry of their orbit and the detector's location and orientation, and the time and phase of the waves at coalescence). This large set of parameters leads to a huge variety of chirplike waveform shapes and a corresponding requirement for a huge number of templates in the search family. On the other hand, for two reasons the number of templates should not be allowed to grow too large: (i) The task of computing the cross-correlations can become excessive [2] and (ii) the probability of a false detection can become excessive. Rough estimates [2,3] suggest that $\sim 10^5 - 10^6$ discrete template shapes might be needed and would be acceptable.

Throughout our analysis and discussion, we assume that the binaries are orbiting around each other in circular orbits when their waves enter the frequency band of the LIGO-VIRGO-GEO detectors. This is justified since long-lived binaries have sufficient time to circularize by radiation reaction, before they reach the LIGO-VIRGO-GEO frequency bands [4] (by contrast with the type of binaries formed by capture events in dense galactic nuclei which might be appropriate sources for the low-frequency space-based Laser Interferometer Space Antenna (LISA) detector [5]).

The most obvious, and perhaps adequate, way to construct a suitable template family is to use approximate waveforms that depend on a small set of parameters related to some special characteristics of the binaries. The simplest such family is the Newtonian family, i.e., the family of waveforms predicted by Newtonian gravity and the quadrupole-moment formalism. These templates (assuming circular orbits) consist of three parameters altogether: the coalescence time t_C, the phase of the waves at coalescence ϕ_C, and a certain combination of the masses, called the *chirp mass*: $\mathcal{M} \equiv (M_1 M_2)^{3/5}/(M_1 + M_2)^{1/5}$. The final coalescence time t_C is a special parameter that can be handled directly as an additive phase factor when computing the cross correlation in the frequency domain [2]. Fortunately only two values of ϕ_C need to be considered, since ϕ_C shows up only as a constant phase in the signal: For convenience $\phi_C = 0$ and $\phi_C = \pi/2$ (see [2]).

As a result, the Newtonian family has only one nontrivial shape parameter: the chirp mass $\mathcal{M}$. The Newtonian family can be handled easily, even with present-day workstations, by spanning the whole range of $\mathcal{M}$'s under consideration with a density $\Delta\mathcal{M}/\mathcal{M}$ of 0.1% [6]. The question that arises is, how adequate are the Newtonian templates for identifying realistic waveforms in the noisy detector output? As a tool for answering this question, we introduce the *fitting factor* (FF) which is a measure of how well any chosen family of templates fits some chosen hypothetical gravitational-wave signal. Several people have used a similar or even the same quantity for the same purpose [7,8], but they have given it other names and have discussed it from other viewpoints.

The noise spectrum of the detector plays a significant role in the FF, since a good resemblance between the template and the incoming waveform is needed only at frequencies where the noise is low. In this paper the "advanced-LIGO-detector" noise spectrum will be used. This spectrum has been introduced by the LIGO team [1] as a guess of what the noise might look like some years after LIGO goes into operation.

As we will show later, the FF is the reduction in signal-to-noise ratio that comes from using some chosen inaccurate family of templates instead of a larger family that includes the true signal. Since the event rate for the true signal scales like the cube of the signal-to-noise ratio, the fractional reduction in event rate due to using the chosen template family is $1-\mathrm{FF}^3$. A value of 0.9 for a family's FF thus means a 27% loss in the event rate. This loss could be recovered by increasing the interferometers' arm length by 10%, but the cost would be roughly 6×10^6 dollars. It should be clear from the numbers that FF values below ~ 0.9 mean that the chosen template family is *inadequate*, and one might want to insist on FF $\gtrsim 0.95$ or even 0.98 when designing a template family.

Several people [7,8] have recently investigated the effectiveness of the Newtonian template family in searches for the nonmodulated waveforms produced by inspiraling binaries with vanishing spins and circular orbits. The numbers obtained in these studies correspond to a FF well below 0.9. I have confirmed these numbers, and I present them together with the results of some additional computations (discussed later in this paper) in Table I. The signals discussed in this table are Newtonian, post^1-Newtonian or post$^{1.5}$-Newtonian approximations to the exact, general relativistic waveforms. (The waveforms have not yet been computed to higher than post$^{1.5}$-Newtonian order, though an ongoing effort [9] should ultimately bring them up to and including post^3-Newtonian order, which is about the accuracy required for LIGO-VIRGO-GEO [10].)

The main conclusion of Table I is that for the post$^{1.5}$-Newtonian signal, with vanishing modulation (because the spin and orbital angular momenta are aligned), the Newtonian template family is completely inadequate. To achieve an acceptable FF $\gtrsim 0.9$ requires the post$^{1.5}$-Newtonian family of templates (templates described by the post$^{1.5}$-Newtonian waveforms with zero spins).

In all previous template investigations, and in all entries in Table I, the binary's spin and orbital angular momenta are assumed to be aligned, or the spins are assumed to vanish, and so the binary does not precess and the waveforms are not modulated. The principal objective of this paper is to study the effects of spin-induced precession and modulation on the acceptability of unmodulated template families. In these modulational studies, as in most previous studies [7,8] (but not all [6]), the discreteness of the template families is ignored; i.e., the chirp mass $\mathcal{M}$ and other parameters that determine the template waveforms are allowed to vary continuously rather than taking on a discrete set of values.

In this continuum approximation, we begin by investigating the detectability of a modulated waveform with the (unmodulated) Newtonian template family. The resulting FF values are unacceptably low, not just because of post-Newtonian effects, but also because of the modulational effects. To rectify this, we introduce the spin-free, unmodulated post$^{1.5}$-Newtonian family described in the previous paragraph, which has four parameters by contrast with three for the Newtonian family. The extra parameter is related to the binary's reduced mass. The

new template family fits better the modulated waveforms than the Newtonian one. From the sets of FF values that we compute, we suspect that an adequate template family, for *almost*, but not quite all binary signals (modulated and unmodulated) that LIGO-VIRGO-GEO seek, will be the four-parameter post^3-Newtonian waveforms of spin-free binaries, waveforms that will likely have been computed within the next ~ 3 yr [9].

The rest of this paper is organized as follows. In Sec. II we briefly review the equations for the spin-induced simple precession and its modulation of the relevant waveforms, based on the stationary phase method, from the work of Apostolatos *et al.* [11]. More specifically, we express the waveforms as Newtonian signals with amplitude and phase modulation. We assume for simplicity that the precessing binaries consist of one spinning object and one nonspinning object; this permits us to use the analytic forms derived in Ref. [11] for the simple precession. This is not a very restrictive assumption since the general case with two spins leads to similar precession trails for the orbital plane. We assume that the spinning object is the more massive one; this maximizes the strength of the precession.

In Sec. III A we define the fitting factor (FF) and show its physical significance as a measure of the reduction of the signal-to-noise ratio due to the use of an inaccurate family of templates that cannot perfectly match the signal. In Sec. III B we derive a simple formula for the FF when the template family is Newtonian and the signal is Newtonian with precession. In Sec. III C we discuss separately the effects of amplitude modulation (AM) and phase modulation (PM) on the fitting factor and show some analytic and numerical examples.

In Sec. IV A we briefly discuss the code we have used to compute the FF and its numerical errors, as well as the difficulties underlying our search for the FF's maximum value over our template family. In Sec. IV B we begin our study of the FF for the Newtonian template family and precessing Newtonian signal by exploring the dependence of the FF on the binary's location on the sky and the orientation of the detector arms. We show that a knowledge of the FF for a binary directly overhead (or underfoot) is adequate to determine the complete distribution of the FF for all other directions to the source. In Sec. IV C we discuss the effect on the FF of the direction of the binary's total angular momentum $\mathbf{J}$, around which the orbital plane precesses. In Sec. IV D we show how the nonrandomly distributed parameters, the binary's masses M_1, M_2 and the opening angle $\hat{\mathbf{L}}\mathbf{S}$ between its orbital and spin angular momenta, affect the FF.

In Sec. V, for a few representative values of these nonrandomly distributed parameters, we compute the probability, over all the random parameters of Secs. IV B, IV C, IV D, to achieve FF values above some critical level. We find that, for a $1.4M_\odot, 1.4M_\odot$ NS-NS binary, with one of the NS's spinning near breakup, the FF is pleasingly large (> 0.9) for most ($\gtrsim 90\%$) of the geometries. But for a $10M_\odot, 1.4M_\odot$ BH-NS binary with the BH spinning at its maximal rate, the FF can be unpleasantly low and is very sensitive to the opening angle $\hat{\mathbf{L}}\mathbf{S}$. For example, for moderate and high values of $\hat{\mathbf{L}}\mathbf{S}$ (above 30°) the FF's are well below 0.9 in more than half of the random geometries.

In Sec. VI we suggest the addition of one more parameter to the Newtonian template family, to improve its ability to detect precessing waveforms. This extra term has the same form as arises from the nonprecessional post^1-Newtonian correction to the waveform's phase, and it turns out to improve substantially the FF values for precessionally modulated Newtonian signals. For the $1.4M_\odot$, $1.4M_\odot$ NS-NS binary, the FF values remain above 0.9 for at least 90% of all the geometries. By contrast, for the BH-NS binary, the FF values still depend strongly on the misalignment angle $\hat{\mathbf{L}}\mathbf{S}$, but now for a 30° angle, there is $\sim 75\%$ probability to get a FF value above 0.9 (an improvement from $< 50\%$).

In Sec. VII we review, in the language of our FF, what other people have already published for the detectability of post-Newtonian nonmodulated signals by various template families. The Newtonian template family is completely inadequate (FF generally well below 0.9). Far better FF's are achieved by a template family based on the waveforms for nonspinning post$^{1.5}$-Newtonian-order binaries.

In Sec. VIII we explore the fitting ability of these post$^{1.5}$-Newtonian templates for post$^{1.5}$-Newtonian signals to which spin-induced modulation has been added. The results were improved at least as much as in Sec. VI, where spin-modulated Newtonian signals and unmodulated post^1-Newtonian templates were considered (i.e., for the NS-NS binary the FF is above 0.9 for at least 90% of all the geometries, and for the BH-NS binary there is a $\sim 75\%$ probability to get a FF value above 0.9 if the misalignment angle is 30°).

Finally, in Sec. IX we summarize our results and suggest future research directions on the issue of search templates for detecting inspiraling binaries.

All of this analysis assumes the noise spectrum of "advanced" high-frequency ground-based LIGO detectors. In the Appendix, we extend the analysis to various kinds of signals and templates in the context of the low-frequency, space-based LISA gravitational-wave detector. The extrapolation to this type of detector and its relevant binary sources (supermassive black holes with smaller-mass black holes or neutron stars) is straightforward, since the corresponding noise spectrum has the same shape as the LIGO noise spectrum, but shifted to much lower frequencies (10^{-4}–1 Hz compared with 10–1000 Hz for LIGO). This similarity suggests the use of the same kind of search templates for LISA as for the ground-based detectors, but with parameters corresponding to much more massive objects.

Throughout we use units where $G = c = 1$.

II. REVIEW OF FORMULAS FOR SIMPLE PRECESSION AND ITS WAVEFORM MODULATION

As was shown in the work of Apostolatos *et al.* [11], a binary consisting of a spinning object with mass M_1 and

spin $\mathbf{S}$, and a nonspinning object M_2 orbiting around each other with angular momentum $\mathbf{L}$ will conserve the angle $\widehat{\mathbf{LS}}$ between $\mathbf{L}$ and $\mathbf{S}$ through the whole inspiral phase. The binary's orbital plane will precess around the total angular momentum $\mathbf{J} = \mathbf{L} + \mathbf{S}$, which remains almost fixed in direction. By using the notation

$$\kappa \equiv \hat{\mathbf{L}} \cdot \hat{\mathbf{S}} , \quad \cos\lambda_L \equiv \hat{\mathbf{L}} \cdot \hat{\mathbf{J}} , \tag{1}$$

the opening angle for the precession of $\hat{\mathbf{L}}$ was shown to evolve due to radiation reaction and hence shrinkage of $\mathbf{L}$ according to

$$\cos\lambda_L(t) = \frac{\mu\sqrt{Mr(t)} + S_{\|}}{\left\{\left[\mu\sqrt{Mr(t)} + S_{\|}\right]^2 + {S_\perp}^2\right\}^{1/2}} . \tag{2}$$

Here carets denote unit vectors (e.g., $\hat{\mathbf{L}} = \mathbf{L}/|\mathbf{L}|$), M and μ are the total and reduced masses, respectively, $r(t)$ is the distance between the two stars, and $S_{\|} \equiv S\kappa$ and $S_\perp \equiv S\sqrt{1-\kappa^2}$ are the components of $\mathbf{S}$ parallel and perpendicular to the angular momentum $\mathbf{L}$, respectively. The evolution of the angular position α of $\hat{\mathbf{L}}$ (see Fig. 1) around the constant $\hat{\mathbf{J}}$ is given by

$$\alpha = \frac{-5\left(1+\frac{3M_2}{4M_1}\right)}{96\mu^3M^3}\left[2Y^{3/2} - 3S_{\|}\left(\mu\sqrt{Mr} + S_{\|}\right)\sqrt{Y}\right.$$

$$\left. -3S_{\|}{S_\perp}^2 \sinh^{-1}\left(\frac{\mu\sqrt{Mr} + S_{\|}}{S_\perp}\right)\right] + \text{const} , \tag{3a}$$

where

$$Y \equiv \mu^2 Mr + 2S_{\|}\mu\sqrt{Mr} + S^2. \tag{3b}$$

Because the computational search for the modulated signal will take place in the frequency domain, it will be useful to know the dependence of the binary's orbital diameter on the frequency f of the gravitational waves:

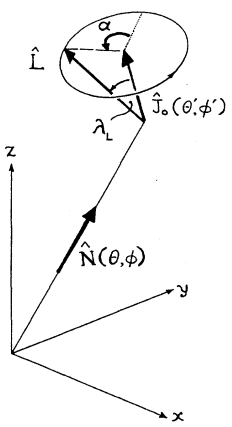

FIG. 1. The geometry for a binary's simple precession relative to an Earth-based detector's Cartesian axes.

$$r = \left(\frac{M}{\pi^2 f^2}\right)^{1/3} . \tag{4}$$

This completes the formulas needed to describe the *simple precession* of the orbital plane of a binary when M_1, M_2, S, κ, and $\hat{\mathbf{J}}$ are given. It should be noted, however, that if the quantity

$$\epsilon = \frac{16}{5}\frac{(M/r)^{3/2}}{\left(1+\frac{3}{4}M_2/M_1\right)\left(1+2\kappa\gamma+\gamma^2\right)} \tag{5}$$

(where $\gamma = S/L$) is *not* $\ll 1$, then all the above expressions for the simple precession break down and instead the binary undergoes a different type of precession, called *transitional precession* [11]. Fortunately (for this paper), this happens only for a tiny, presumably rare range of parameters, $\hat{\mathbf{L}} \cdot \hat{\mathbf{S}} \lesssim -0.94$ ($\widehat{\mathbf{LS}} \gtrsim 160°$), and a rather restrictive combination of masses (see Fig. 10 of Ref. [11]). In the following examples we avoid any situation where transitional precession is involved, since no analytic expressions exist then.

We now move on to present the equations that describe the modulation of the waves due to simple precession. We write down directly the Fourier transform $\tilde{h}(f)$ of the modulated waveforms, since our calculations will be performed in the frequency domain. As shown in Eq. (38) of Ref. [11], by following the stationary phase method this $\tilde{h}(f)$ is given by

$$\tilde{h}(f) \approx \frac{1}{2}\Lambda(t)\tilde{h}_C(f) + \frac{1}{4\pi i}\frac{d\Lambda}{dt}\left[\frac{d\tilde{h}_C(f)}{df} - 2\pi i t\tilde{h}_C(f)\right] \tag{6}$$

for positive f, and the complex conjugate of this for negative f. Whenever we write t we simply mean $t(f)$, the time at which the carrier frequency is f, given by

$$t(f) = t_C - 5(8\pi f)^{-8/3}\mathcal{M}^{-5/3} . \tag{7}$$

In Eq. (6), $\tilde{h}_C(f)$ is the Fourier transform of the unmodulated "carrier" signal,

$$h_C(t) \equiv \frac{2M_1M_2}{D\,r(t)}e^{-2i\Phi_C(t)} , \tag{8}$$

where $\Phi_C(t) = \int \Omega dt$ is the carrier phase, Ω is the orbital angular velocity, and D is the distance to the binary. This Fourier transform is

$$\tilde{h}_C(f) = \text{const} \times f^{-7/6}e^{i\left[2\pi f t_C - \phi_C + \frac{3}{4}(8\pi\mathcal{M}f)^{-5/3}\right]}, \tag{9}$$

where the "const" represents everything that does not depend on frequency, such as the geometry, the masses, etc.; ϕ_C, not to be confused with Φ_C, stands for the phase of the waveform at coalescence, t_C for the time of coalescence, and $\mathcal{M}$ for the *chirp mass*. $\Lambda(t)$ in Eq. (6) is the modulation factor defined as

$$\Lambda(t) \equiv \text{AM} \times \text{PM} , \tag{10}$$

where AM and PM are the following *amplitude modula-*

tion factor and *phase modulation factor*,

$$\mathrm{AM} = \{4[\hat{\mathbf{L}}\cdot\hat{\mathbf{N}}]^2 {F_\times}^2(\theta,\phi,\psi) + [1+(\hat{\mathbf{L}}\cdot\hat{\mathbf{N}})^2]^2 {F_+}^2(\theta,\phi,\psi)\}^{1/2} , \tag{11}$$

$$\mathrm{PM} = e^{-i[2\delta\Phi(t)+\varphi(t)]} . \tag{12}$$

Here, as before, $t = t(f)$, and

$$\varphi = \arctan\left(\frac{2\hat{\mathbf{L}}\cdot\hat{\mathbf{N}}\, F_\times(\theta,\phi,\psi)}{[1+(\hat{\mathbf{L}}\cdot\hat{\mathbf{N}})^2]F_+(\theta,\phi,\psi)}\right) , \tag{13}$$

$$\delta\Phi(t) = -\int_{\hat{\mathbf{L}}}^{\hat{\mathbf{L}}_{\mathrm{final}}} \left(\frac{\hat{\mathbf{L}}\cdot\hat{\mathbf{N}}}{1-(\hat{\mathbf{L}}\cdot\hat{\mathbf{N}})^2}\right)(\hat{\mathbf{L}}\times\hat{\mathbf{N}})\cdot d\hat{\mathbf{L}} . \tag{14}$$

The two phases in Eqs. (13), (14) represent phase modulations that have different physical origins: φ arises from changes in the polarization axes due to precession of the orbital plane, and $\delta\Phi$ is something similar to the Thomas precession of the electron's spin in a semiclassical model of the hydrogen atom. The rest of the parameters in Eqs. (11)–(14) are connected to the orientation of the detector and the direction to the binary. Thus $\hat{\mathbf{N}}$ is the unit vector pointing to the source and θ and ϕ are its spherical polar coordinates (see Fig. 1), F_+ and $F_\times$ are the detector's "beam-pattern" coefficients given by

$$F_+(\theta,\phi,\psi) = \frac{1}{2}(1+\cos^2\theta)\cos 2\phi\cos 2\psi - \cos\theta\sin 2\phi\sin 2\psi , \tag{15a}$$

$$F_\times(\theta,\phi,\psi) = \frac{1}{2}(1+\cos^2\theta)\cos 2\phi\sin 2\psi + \cos\theta\sin 2\phi\cos 2\psi , \tag{15b}$$

and ψ is the polarization angle given up to an arbitrary multiple of π by

$$\psi = \arctan\left(\frac{\hat{\mathbf{L}}\cdot\hat{\mathbf{p}} - (\hat{\mathbf{L}}\cdot\hat{\mathbf{N}})(\hat{\mathbf{p}}\cdot\hat{\mathbf{N}})}{\hat{\mathbf{N}}\cdot(\hat{\mathbf{L}}\times\hat{\mathbf{p}})}\right) , \tag{16}$$

where $\hat{\mathbf{p}}$ is the normal to the detector plane.

By combining Eqs. (6), (9), (10), (12), $\tilde{h}(f)$ turns out to be

$$\tilde{h}(f) \approx \frac{1}{2}\tilde{h}_C(f)\times\mathrm{AM}\times\mathrm{PM} \times\left[1+\frac{7}{12\pi f}(2\delta\dot{\Phi}+\dot{\varphi}) + \frac{7i}{12\pi f}\frac{\dot{\mathrm{AM}}}{\mathrm{AM}}\right] , \tag{17}$$

where an overdot represents d/dt. Expressions for AM and PM can be read from Eqs. (11), (12). The quantity in the square brackets in Eq. (17) can be approximated by 1 since the remaining terms are corrections of order (orbital period)/(precession period) $\approx \Omega_p/\pi f$ [see Eq. (42) of Ref. [11]], which is a very small quantity except maybe at high frequencies near the final stages of inspiral, where the detectors are almost "deaf" due to large shot noise.

III. FITTING FACTOR (FF)

A. Definition and physical significance

Let us imagine a detector receiving a gravitational signal from a precessing binary with a waveform represented by $W(t)$. Then because of the detector's noise $n(t)$, the output $s(t)$ of the detector will be

$$s(t) = W(t) + n(t) . \tag{18}$$

If we had used the exact waveform $W(t)$ as our search template, then we would have achieved the highest possible signal-to-noise ratio, given by Eq. (2.5) of Ref. [12];

$$\left(\frac{S}{N}\right)_{\max} = (W \mid W)^{1/2} , \tag{19}$$

where the inner product of two waveforms $(h_1 \mid h_2)$ is defined by Eq. (2.3) of Ref. [12]:

$$(h_1 \mid h_2) = 2\int_0^\infty \frac{\tilde{h}_1^*(f)\tilde{h}_2(f) + \tilde{h}_1(f)\tilde{h}_2^*(f)}{S_n(f)}\, df . \tag{20}$$

Here $S_n(f)$ is the spectral density of the detector's noise. Henceforth we will assume for $S_n(f)$ the following analytic fit to the "advanced" LIGO noise spectrum, which has been published by the LIGO team as an estimate of what might be achieved some years after LIGO turns on (see Refs. [1,12]):

$$S_n(f) = \begin{cases} \infty & \text{for } f < 10 \text{ Hz}, \\ S_0\left[\left(\frac{f_0}{f}\right)^4 + 2\left(1+\left(\frac{f}{f_0}\right)^2\right)\right] & \text{for } f > 10 \text{ Hz}, \end{cases} \tag{21}$$

where $S_0 = 0.6\times 10^{-48}\ \mathrm{Hz}^{-1}$ and $f_0 = 70$ Hz.

The signal-to-noise ratio will be reduced below $(S/N)_{\max}$ whenever the template is not the exact waveform but some other approximate one. In this paper we are interested in searches performed with some family of templates $T_{\lambda_1,\lambda_2,\ldots}(t)$ that depend on a set of parameters $\lambda_1,\lambda_2,\ldots$. Then by definition the signal to noise achieved in the search will be

$$\left(\frac{S}{N}\right) = \max_{\lambda_1,\lambda_2,\ldots} \frac{(s \mid T_{\lambda_1,\lambda_2,\ldots})}{\mathrm{rms}\,(n \mid T_{\lambda_1,\lambda_2,\ldots})} . \tag{22}$$

For an ensemble of realizations of the detector noise, the expectation values of $(n \mid T_{\lambda_1,\lambda_2,\ldots})$ and $(n \mid T_{\lambda_1,\lambda_2,\ldots})$ $(n \mid$

$T_{\lambda_1,\lambda_2,\ldots})$ are 0 and $(T_{\lambda_1,\lambda_2,\ldots} \mid T_{\lambda_1,\lambda_2,\ldots})$, respectively. Thus the ensemble-averaged signal-to-noise ratio turns out to be

$$\left(\frac{S}{N}\right) = \max_{\lambda_1,\lambda_2,\ldots} \frac{(W \mid T_{\lambda_1,\lambda_2,\ldots})}{\sqrt{(T_{\lambda_1,\lambda_2,\ldots} \mid T_{\lambda_1,\lambda_2,\ldots})}} = \left[\max_{\lambda_1,\lambda_2,\ldots} \frac{(W \mid T_{\lambda_1,\lambda_2,\ldots})}{\sqrt{(T_{\lambda_1,\lambda_2,\ldots} \mid T_{\lambda_1,\lambda_2,\ldots})(W \mid W)}}\right] \left(\frac{S}{N}\right)_{\max} . \tag{23}$$

We give the name *fitting factor* (FF) to the reduction in signal to noise that results from using the chosen template family, rather than the true signal W, in the search:

$$\mathrm{FF} \equiv \max_{\lambda_1,\lambda_2,\ldots} \frac{(T_{\lambda_1,\lambda_2,\ldots} \mid W)}{\sqrt{(T_{\lambda_1,\lambda_2,\ldots} \mid T_{\lambda_1,\lambda_2,\ldots})(W \mid W)}} . \tag{24}$$

This FF or its square root is a quantity that has already been used by various authors (see [7,8]) as a measure of the adequateness of a template family, but previous discussions have not shown explicitly how this intuitively well-formed function is connected with detectability. Previously this FF has sometimes been called the "correlation," a name that is often used in so many different ways that we prefer to avoid it. The new name we have adopted comes from the fact that, by maximizing the quantity in Eq. (24), we essentially adjust the parameters of the templates to best *fit* the true waveform.

B. Form of the FF for the Newtonian template family searching for a precessionally modulated Newtonian signal

In this section we will construct an explicit expression for the FF when a "Newtonian template family" is used to search for the modulated Newtonian waveforms of Sec. II.

The *Newtonian template family* has been introduced and studied previously by a number of researchers [7,8]. Each Newtonian template is the waveform predicted in the Newtonian, quadrupole moment approximation, for some circular, inspiraling binary, and it therefore has the same form $h_C(t)$ [or $\tilde{h}_C(f)$] as the carrier signal (8). Of course the parameters const, t_C, ϕ_C, and $\mathcal{M}$ of the Newtonian template are not in general the same as these of the "true," modulated signal's carrier. Rather, the template parameters must be adjusted to make the Newtonian template resemble as well as possible the modulated waveform.

By using Eq. (17), the FF for a Newtonian filter takes the form

$$\mathrm{FF} = \max_{\Delta t_C,\Delta\phi_C,\Delta(\mathcal{M}^{-5/3})} \frac{\mathrm{Re}\left[\int_0^\infty df \frac{f^{-7/3}}{S_n(f)} e^{i\Psi(f)} \mathrm{AM} \times \mathrm{PM}\right]}{\sqrt{\left[\int_0^\infty df \frac{f^{-7/3}}{S_n(f)}\right]\left[\int_0^\infty df \frac{f^{-7/3}}{S_n(f)} (\mathrm{AM})^2\right]}} , \tag{25a}$$

$$\Psi(f) = 2\pi f \Delta t_C - \Delta\phi_C + \frac{3}{4}(8\pi f)^{-5/3} \Delta(\mathcal{M}^{-5/3}) , \tag{25b}$$

and $\Delta t_C, \Delta\phi_C$, and $\Delta(\mathcal{M}^{-5/3})$ are the differences in the parameters between a chosen template and the modulated signal's carrier. Note that all multiplicative factors not depending on frequency, such as the distance to the binary, have been canceled out because of the specific form of the FF, which automatically normalizes the template and the signal. Fortunately, one of the maximization parameters $\Delta\phi_C$ affects the FF value trivially, and there is no need to fine-tune it. To maximize the FF over $\Delta\phi_C$, one need only compute the values for the FF with $\Delta\phi_C = 0$ and $\Delta\phi_C = \pi/2$ and then add them in quadrature. Therefore Eq. (25a) for the FF simplifies to

$$\mathrm{FF} = \max_{\Delta t_C,\Delta(\mathcal{M}^{-5/3})} \frac{\left|\int_0^\infty df \frac{f^{-7/3}}{S_n(f)} e^{i\Psi(f)} \mathrm{AM} \times \mathrm{PM}\right|}{\sqrt{\left[\int_0^\infty df \frac{f^{-7/3}}{S_n(f)}\right]\left[\int_0^\infty df \frac{f^{-7/3}}{S_n(f)} (\mathrm{AM})^2\right]}} , \tag{26a}$$

where $\Psi(f)$ is the same as in Eq. (25b) but with $\Delta\phi_C$ eliminated,

$$\Psi(f) = 2\pi f \Delta t_C + \frac{3}{4}(8\pi f)^{-5/3} \Delta(\mathcal{M}^{-5/3}) . \tag{26b}$$

This is the expression that we have used in a computer code, described later in Sec. IV A, to compute the FF for various modulated signals. In addition to the obvious parameters in the FF, shown explicitly in Eqs. (26a), (26b), there are a few others hidden inside the AM, PM

functions: the four angles θ, ϕ, w, g (see Fig. 3 below) defining the orientation and direction of the binary on the sky and the direction of its total angular momentum, the angle $\cos^{-1}\kappa$ between the orbital angular momentum and the spin, the masses M_1 and M_2 of the two objects, and the magnitude S of the spin.

C. How do the amplitude and phase modulation affect the FF?

Before we present the numerical results that we have obtained for the FF in various cases, it will be helpful to seek some intuition into the roles that AM and PM play in the value of the FF. We will begin with the effect of AM alone without any phase modulation. For vanishing PM, the FF takes a much simpler form than Eqs. (26):

$$\mathrm{FF} = \frac{\int_0^\infty df \frac{f^{-7/3}}{S_n(f)} \mathrm{AM}}{\sqrt{\left[\int_0^\infty df \frac{f^{-7/3}}{S_n(f)}\right]\left[\int_0^\infty df \frac{f^{-7/3}}{S_n(f)} (\mathrm{AM})^2\right]}} . \quad (27)$$

The $e^{i\Psi(f)}$ term has disappeared because, with PM=0, the FF is maximized by $\Delta t_C = \Delta(\mathcal{M}^{-5/3}) = 0$. It is straightforward to see that if AM were also a constant (no amplitude modulation), the FF would be 1, meaning no signal-to-noise reduction at all. But what if the amplitude has a large depth of modulation such as the $A_{\times'}$ in Fig. 6 of Ref. [11]? For the sake of simplicity, we will assume that the form of AM during one binary precession is approximately given by AM=$|\sin(kf)|$ for some k, which very much resembles the plot of $A_{\times'}$ in Fig. 6 of Ref. [11]. Bearing then in mind that $f^{-7/3}/S_n(f)$ changes rather slowly during one precession (see Fig. 2 of Ref. [12]), one can infer that

$$\mathrm{FF} \approx \frac{\int_0^\pi \sin(x)\, dx}{\sqrt{\left[\int_0^\pi dx\right]\left[\int_0^\pi \sin^2(x)\, dx\right]}} = \frac{2\sqrt{2}}{\pi} = 0.900 . \quad (28)$$

Of course this is a lower limit on the FF due to AM, since it corresponds to the deepest possible modulation.

To get a feeling for *realistic* minimum values of the FF due to AM, consider a binary with a maximally spinning $10M_\odot$ black hole and a nonspinning $1.4M_\odot$ neutron star with an $\hat{\mathbf{L}}\mathbf{S}$ angle of 30° and choose its location and orientation to produce the worst possible amplitude modulation. Then the FF with no PM turns out to be 0.907, in very good agreement with our rough approximate value of Eq. (28).

Turn, now, from AM with vanishing PM to PM with vanishing AM. The analysis in this case is somewhat more complicated, since the two parameters $\Delta t_C, \Delta(\mathcal{M}^{-5/3})$ have to be suitably tuned, to cancel out as well as possible the effects of φ, and $\delta\Phi$ given in Eqs. (13), (14). It can be easily verified that a perfect cancellation is not possible: The simple frequency dependence of $\Psi(f)$ [Eq. (26b)] *cannot* perfectly correct for the oscillating behaviors of φ and $\delta\Phi$. If the amplitude of phase modulation is high, then $\Psi(f)$ is totally unable to keep the FF at high levels (> 0.9).

There is another effect (for some cases the main effect) that causes PM to produce low values of the FF. As has been shown in Eq. (45) of Ref. [11], the number of precessions for the two extreme cases $L \gg S$, $S \gg L$ can be inferred from the following expression for the precession angle:

$$\frac{\alpha(f)}{2\pi} \approx \begin{cases} 11\left(1+\frac{3M_2}{4M_1}\right)\frac{10M_\odot}{M}\frac{10\mathrm{Hz}}{f} & \text{for } L \gg S, \\ 1.9\left(1+\frac{3M_2}{4M_1}\right)\frac{M_1}{M_2}\frac{S}{M_1^2}\left(\frac{10M_\odot}{M}\frac{10\mathrm{Hz}}{f}\right)^{2/3} & \text{for } S \gg L. \end{cases} \quad (29)$$

Now, in the case of secular evolution of φ (see Fig. 7 of Ref. [11]), φ varies like $\alpha(f)$ on top of the additional oscillation we talked about in the last paragraph. But the frequency dependence of $\alpha(f)$ is very different ($\propto f^{-2/3}$ to f^{-1}) from that of $\Psi(f)$. Therefore, $\Psi(f)$ cannot follow the evolution of $\varphi + 2\Delta\Phi$ for long frequency intervals, and the FF remains at low levels.

Finally, there is a third PM effect that can lead to low FF values. If the PM changes behavior, from oscillatory to secular or conversely, especially at a frequency near $\sim$ 50 Hz where $f^{-7/3}/S_n(f)$ is maximal (see Fig. 2 of Ref. [12]), then $\Psi(f)$ can only attempt to follow the PM evolution during *one* of the two evolution phases; it will fail during the other. This leads to even lower values of the FF. Later on, in Sec. IV, we will check with realistic examples how important these three factors are in lowering the FF and what are the chances for each one of them to play an important role.

For the moment, we will give an example of the FF due to PM alone. For the same BH-NS binary as we discussed a few paragraphs above, when we were examining the effect of the AM on the FF, the lowest value the FF can take for the worst kind of PM is 0.564. This is much lower than the worst FF for the AM alone. It should be noted that the FF values due to PM alone and AM alone cannot be trivially combined to obtain the FF value when both PM and AM are present. For instance, for the above example, where PM alone gives FF=0.564, if the AM alone had been used, then the FF would have been 0.922, but with both AM and PM on, the FF would have been 0.653. Instead of driving the FF to lower values (below 0.564), the AM effect has reduced the bad behavior of the PM effect by strongly suppressing some parts of deep PM modulation. But this is not a general rule. Sometimes AM combines with PM constructively and sometimes destructively.

IV. NUMERICAL INVESTIGATIONS OF THE FF

A. Numerical code

The code written to compute the FF is based on Eqs. (26a), (26b). The integrands are numerically integrated from 10 Hz up to the frequency of the final stable orbit, 4383.45 $(M_\odot/M)$ Hz. Actually this upper limit is rather unimportant for binaries with small total mass ($< 30M_\odot$) because the detector's high shot noise $S_n(f)$ at high frequencies strongly suppresses the integrand. The number of steps used is such that the precession angle α does not change by more than 0.1 rad in each step; this keeps the error in the calculated FF smaller than 10^{-3} and therefore negligible since we compute the FF only to three significant digits.

We have also checked the error due to approximating the square brackets in Eq. (17) by unity. As we expected, the extra factors next to the 1 change the FF by a tiny amount ($< 10^{-4}$) even for rapidly modulated phases and amplitudes.

The only difficulty in computing the FF is to guess the right pair of parameters $\Delta t_C, \Delta(\mathcal{M}^{-5/3})$ that produces the maximum in Eqs. (26a), (26b). Of course, the code is able to climb up at a maximum, but there is no guarantee that this is *the global maximum.* The form of the function to be maximized on the two-parameter Δt_C, $\Delta(\mathcal{M})^{-5/3}$ space is very complicated; see Fig. 2.

We have roughly guessed the region of the global maximum by computing the average value of d(modulating phase)$/df$ around 50 Hz and adjusting the parameters of $d\Psi(f)/df$ so that the two slopes are almost opposite. Then, starting from this point the code climbs up to the neighboring maximum. By searching a little bit around this peak we can be quite sure that it is the highest peak.

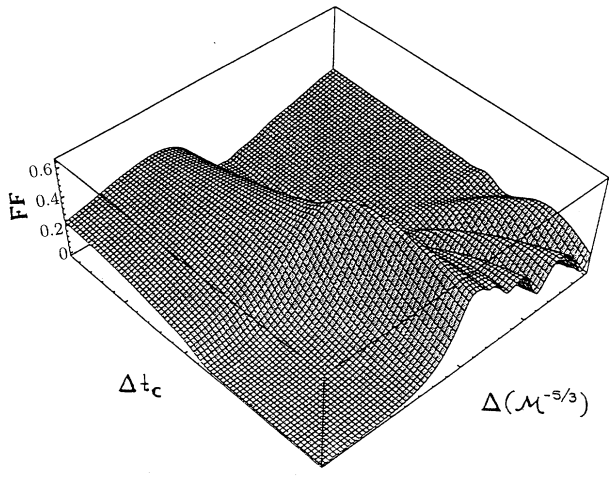

FIG. 2. This is an example of the complicated landscape of the FF on the parameter space of $\Delta t_C, \Delta(\mathcal{M}^{-5/3})$ where many local maxima can be observed. The geometry used here is the one that provided the overall lowest FF value for the case of a maximally spinning $10M_\odot$ black hole and a $1.4M_\odot$ neutron star with $\hat{\mathbf{L}}\mathbf{S} = 30°$.

This procedure becomes more complicated in cases like the one where PM changes behavior at some frequency. Then, there may be more than one candidate place for a global maximum. In the examples that follow we have carefully examined all such candidate places.

It is worthwhile to note that the improved template families we introduced in Secs. VI and VII produce lower values of $|\Delta t_C|$, $|\Delta(\mathcal{M}^{-5/3})|$ than the Newtonian family because the extra parameter itself corrects for PM and AM.

Throughout, we have used a grid on the two-parameter space with a spacing of 1 msec for Δt_C and $2 \times 10^{-5} M_\odot^{-5/3}$ for $\Delta(\mathcal{M}^{-5/3})$. This choice is such that the difference for two nearby grid points in the overall change of $\int d\Psi(f)$, over the band of low detector noise (10–100 Hz), is less than 1 rad. Hence the FF changes very smoothly from point to point.

B. Dependence of the FF on the direction to the binary

In order to study the dependence of the FF on the binary's direction we performed the following search. We assumed that the merging compact binary is located directly above the North Pole of the Earth (of course this choice is only a matter of convention since any other point on Earth would be equivalent). We fixed the direction of the binary's total angular momentum $\mathbf{J}$ and let it precess. Then we filled the whole Earth's surface with identical detectors having the same noise spectrum, described by Eq. (21), and computed the FF for their outputs.

There are three angles related to the location of the detector: the standard θ' and ϕ' spherical coordinates related to the geographic longitude and latitude of the detector's location [not to be confused with the angles θ and ϕ used in Eqs. (15a), (15b)] and an angle w defining the orientation of its arms. In the following we define w to be the angle that one has to rotate the detector on the Earth's surface, for the arms to coincide with the local parallel and meridian (see Fig. 3). Note that w is only defined modulo $\pi/2$ due to the quadrupolar behavior of gravitational waves.

By keeping w fixed and moving the "rotated" detector around the Earth, we notice the following features of the FF. (i) The FF has the same form, as a function of longitude at any latitude, but with some shift γ that depends on the latitude and on the rotation angle w:

$$FF(\theta', \phi', w) \cong FF(\theta' = 0, \phi' + \gamma, w) \,, \tag{30a}$$

where

$$\gamma = \gamma(\theta', w) \,. \tag{30b}$$

This dependence is depicted in Fig. 4 for three different θ' values. It can be explained by the following argument. If the detector's plane is not perpendicular to the waves' propagation direction, then the signal is the same as if the two arms were the projections of the original ones on the plane perpendicular to the propagation direction. The equivalent arms, orthogonal to the direction of the binary, are no longer equal to each other and they form

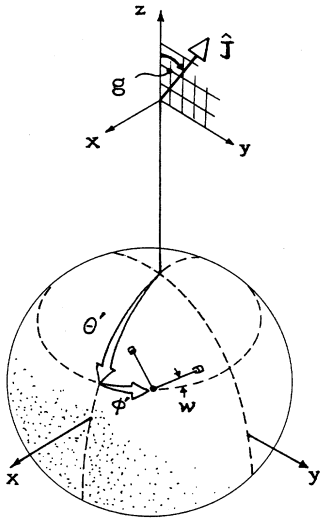

FIG. 3. This is the geometry that we have used to investigate the dependence of the FF on the various random angles θ', ϕ', w, g.

some angle between 90° and 180°. If we now lengthen the shorter arm to give them equal lengths and move them by equal amounts toward the bisector to make them perpendicular, we will change the linear combination of $h_+(t)$ and $h_\times(t)$ (the two waveforms) that they measure, but this change is not important because we could get all the different combinations of polarizations, even with orthogonal detectors (detectors at the North Pole in our case) by rotating the detector in its plane. (ii) For the two special cases of detectors at the North Pole (and equivalently at the South Pole) and at the equator it is easy to verify analytically that

$$\mathrm{FF}(\theta'=0,\phi'_1,w_1=0)=\mathrm{FF}(\theta'=0,\phi'_2=0,w_2=\phi'_1) \tag{31a}$$

and

$$\mathrm{FF}(\theta'=\pi/2,\phi'_1,w_1)=\mathrm{FF}(\theta'=0,\phi'_1,w_2=0)\,. \tag{31b}$$

The former corresponds to the fact, easily seen in Fig. 4, that for $\theta'=0$ the detector's orientation depends only on $\phi'+w$ and not separately on ϕ' and w. The latter can be easily understood, since at the equator a detector is equivalent to a one-arm detector perpendicular to the incoming waves.

This dependence of the FF on the location of the detector on Earth simplifies our investigation of the FF a lot. Equation (30a) makes it possible to restrict ourselves to detectors orthogonal to the propagation direction (detectors at the North Pole) without any loss of generality.

C. Dependence of the FF on the direction of the binary's total angular momentum J

We assume, now, that the binary is overhead at the detector and we move the total angular momentum **J** around to see how its direction $\hat{\mathbf{J}}$ affects the FF.

Recall that the modulational phase is the sum of two terms, $\mathrm{PM}=e^{-i[2\delta\Phi(t)+\varphi(t)]}$ [cf. Eq. (12)]. From Eq. (65) of Ref. [11] we know that during one precession $\delta\Phi$ changes by

$$\int_0^{2\pi}\frac{d\,\delta\Phi}{d\alpha}\,d\alpha=\begin{cases}-2\pi\cos\lambda_L & \text{if } |\hat{J}_0\cdot\hat{L}|<|\hat{J}_0\cdot\hat{N}|,\\ 2\pi(-\cos\lambda_L+1) & \text{if } \hat{J}_0\cdot\hat{L}>|\hat{J}_0\cdot\hat{N}|,\\ 2\pi(-\cos\lambda_L-1) & \text{if } \hat{J}_0\cdot\hat{L}<-|\hat{J}_0\cdot\hat{N}|.\end{cases} \tag{32}$$

As for φ, its evolution can be deduced using an intuitive tool introduced in Ref. [11], the *cell diagram* (which is reproduced in Fig. 5). There are six special "singular"

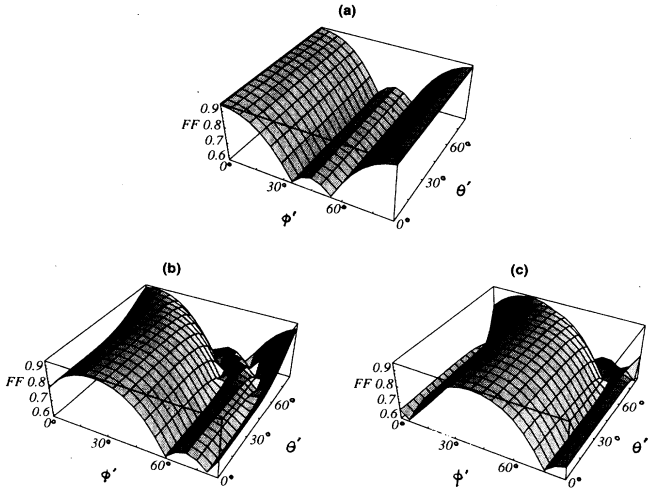

FIG. 4. This is a series of 3 three-dimensional plots showing the FF for a binary of fixed orientation as one moves a detector on the Earth's surface keeping w fixed. (a) $w=0°$, (b) $w=25°$, (c) $w=40°$. The plots verify Eqs (30a), (30b), (31a), (31b).

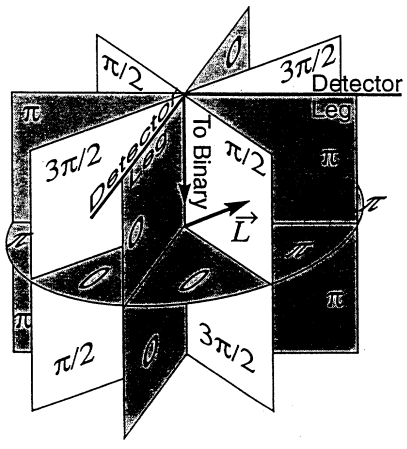

FIG. 5. This *cell diagram*, reproduced from Ref. [11], is a useful tool for understanding how the phase φ evolves while $\hat{\mathbf{L}}$ precesses, for a detector positioned as shown in the diagram. Each wall in the diagram is labeled by the value that φ takes when $\hat{\mathbf{L}}$ lies in that wall. The lines at which black and white walls intersect are singular directions; when $\hat{\mathbf{L}}$ passes near such a line, φ changes rapidly.

directions in the cell diagram: the six intersections of the black and white cell walls. If the binary's precession cone (the cone on which its orbital angular momentum $\hat{\mathbf{L}}$ precesses) encloses one of the singular directions, then φ evolves secularly; otherwise, it oscillates. We expect φ to behave in the most irregular way and thus cause the FF to assume its lowest values for the cases where $\hat{\mathbf{L}}$'s spiraling precession barely touches one of these singular directions at a frequency near 50 Hz, where $f^{-7/3}/S_n(f)$ is maximum (see Fig. 6).

Actually, for the two singular directions where φ changes by 4π with each precession that encloses them, $2\,\delta\Phi$ changes by $-4\pi\cos\lambda_L$ (which is $\simeq -4\pi$ if $\hat{\mathbf{LS}}$ is small), thus moderating the total phase modulation. Correspondingly, as we will see later, these two directions produce fairly high values for the FF, when $\hat{\mathbf{LS}}$ is small.

By contrast, for the other four singular directions, around which φ changes by 2π with each precession, $2\,\delta\Phi$ changes only by $4\pi(1-\cos\lambda_L)$, a small angle if the opening angle $\hat{\mathbf{LS}}$ is small. Thus these four directions will typically produce the lowest values of the FF.

It should be emphasized that it is *not* $\hat{\mathbf{J}}$ itself that leads to low FF values by pointing along these singular

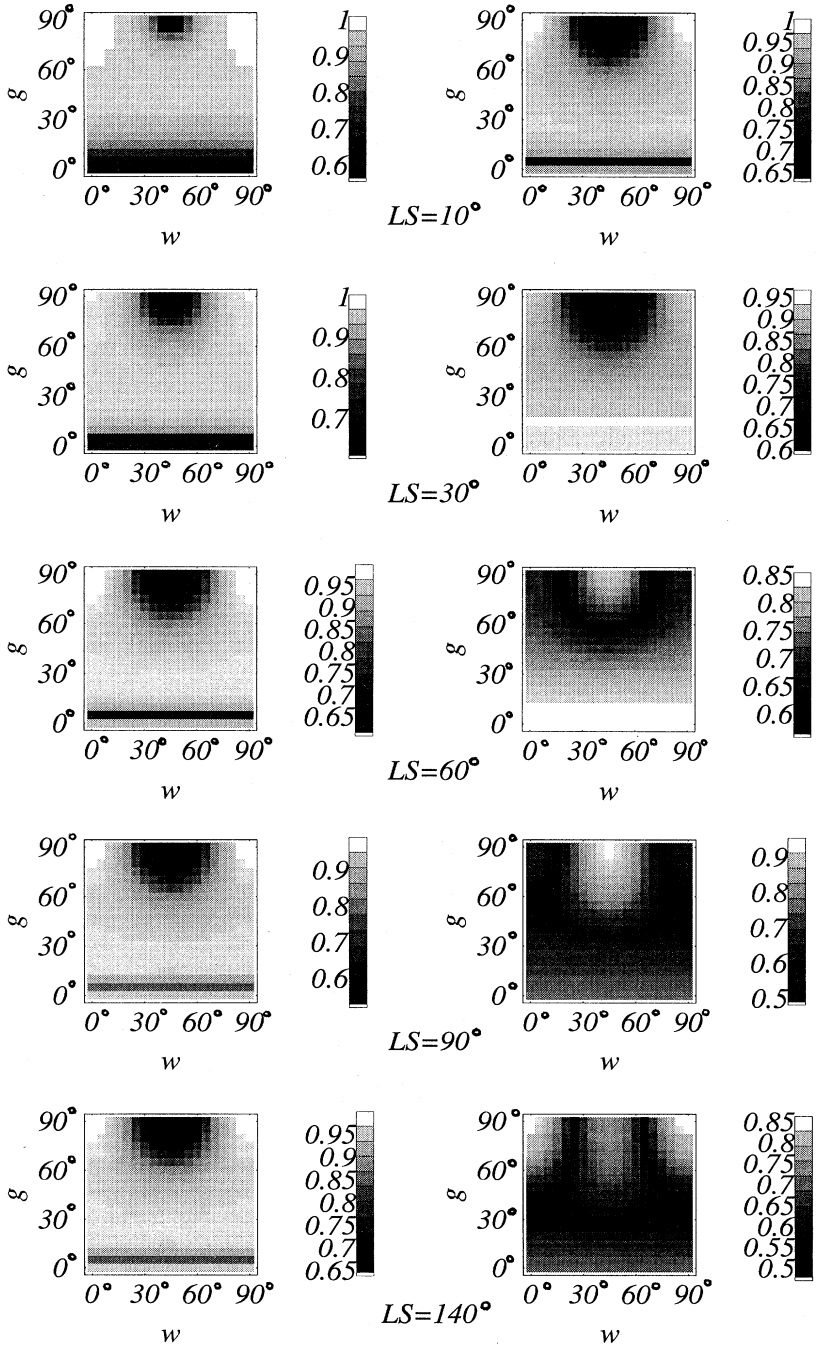

FIG. 6. This is a series of density plot diagrams showing the FF distribution in a grey scale (black represents the lowest values) for a detector at the North Pole as one rotates its arms (variable w) and changes the inclination g of the binary's total angular momentum $\mathbf{J}$ to the z axis (the Earth's rotation axis) while keeping $\mathbf{J}$ in the y-z plane (see Fig. 3). We have arranged the figures in pairs. The left column corresponds to a $1.4M_\odot$, $1.4M_\odot$ NS-NS binary and the right column to a $10M_\odot$, $1.4M_\odot$ BH-NS binary. For both types of binaries the more massive object is maximally spinning ($S_i = M_i^2$). The ring with the low FF around the singular direction ($g = 90°$, $w = 45°$) can be easily recognized. Actually only one-eighth of the whole (g, w) space is displayed here since the same pattern is repeated.

directions, but $\hat{\mathbf{L}}$. Thus, to produce low FF's $\hat{\mathbf{J}}$ should find itself in ringlike areas around these singular points; see Fig. 6.

The situation is much more complicated if the opening angle $\hat{\mathbf{L}}\hat{\mathbf{S}}$ is big than if it is small (but excluding the extreme value of $\approx 180°$ which would lead to transitional precession). In this case the cone of $\hat{\mathbf{L}}$ can encompass more than one singular direction, leading to multiple behavior of the phase evolution and low values of the FF.

In general in the parameter space $[\Delta t_C, \Delta(\mathcal{M}^{-5/3})]$ there are at most as many candidate regions, for expression (25a) for the FF to acquire its global maximum, as the number of singular directions encompassed by the cone of $\hat{\mathbf{L}}$. This happens because, when the evolving precession cone passes through each of the singular directions, the behavior of the phase evolution changes. This information enables us to initiate our numerical search for the FF for various geometries.

D. Dependence of the FF on the masses and the $\hat{\mathbf{L}}\hat{\mathbf{S}}$ angle

Up to this point, we have investigated the dependence of the FF on all the randomly distributed variables defining the geometry of the source-detector system. These are the variables over which we must average to obtain a probabilistic picture of the FF. In the present section, we discuss the effect of the other, nonrandomly distributed, variables M_1, M_2, S, and $\hat{\mathbf{L}}\hat{\mathbf{S}}$. In the following, as in Sec. IV C, we assume that the larger mass is maximally spinning:

$$S = M_1^2 \,. \tag{33}$$

As we showed in Sec. IV C the FF value depends greatly on the opening angle λ_L of the precession cone, and the singular points it encompasses. The angle λ_L itself is a function of the binary's masses, the $\hat{\mathbf{L}}\hat{\mathbf{S}}$ angle, and the gravity wave frequency [cf. Eqs. (2), (4)]. It is easy to show that

$$\frac{L}{S} = 40.088 \left(\frac{M_2}{M_1}\right) \left(\frac{M}{M_\odot}\frac{f}{\mathrm{Hz}}\right)^{-1/3} . \tag{34}$$

From Eq. (2) with $L = \sqrt{Mr}$ we see that the opening angle λ_L is larger if L/S is lower, i.e., if the total mass M is higher and the ratio of masses is lower [Eq. (34)]. Restricting ourselves to our two typical combinations of masses, one with a $10M_\odot$ black hole and a $1.4M_\odot$ neutron star and the other with two $1.4M_\odot$ neutron stars, we can see that in the NS-NS case the λ_L opening angles are much smaller than in the BH-NS case; cf. Fig. 7. Hence we expect, and it is true as we shall see in examples in Sec. V, that the NS-NS binaries produce overall higher values of the FF than NS-BH or BH-BH binaries with unequal masses.

Of course the $\hat{\mathbf{L}}\hat{\mathbf{S}}$ angle plays also a crucial role. If $\hat{\mathbf{L}}\hat{\mathbf{S}}$ is small the values of the FF stay at a high level for most of the various geometries, whatever the masses may be.

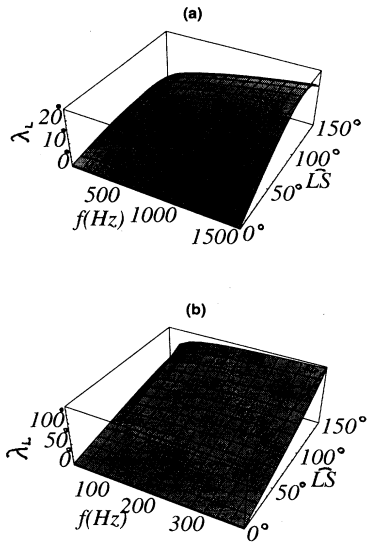

FIG. 7. (a) This three-dimensional plot shows how the opening angle λ_L of $\hat{\mathbf{L}}$ changes with frequency (from 10 Hz up to the frequency of the last stable orbit) for various $\hat{\mathbf{L}}\hat{\mathbf{S}}$ angles, for two representative binaries: (a) a $1.4M_\odot$, $1.4M_\odot$ NS-NS binary with one of the stars maximally rotating, $S_i = M_i^2$; (b) a $10M_\odot$, $1.4M_\odot$ BH-NS binary with the black hole maximally rotating.

V. DETECTABILITY OF PRECESSING BINARIES

We have thoroughly analyzed how the various random variables, such as the position on the sky and the orientation of the binary's plane, affect the FF values. We have also checked how the nonrandom variables such as the masses and the $\hat{\mathbf{L}}\hat{\mathbf{S}}$ angle affect the worsening or improvement of the FF. But ultimately what is important is the probability of detecting these modulating signals. In this spirit, for a number of typical values of the nonrandom parameters, we have integrated all the random variables to investigate what is the probability to have a FF value above some level and therefore to be able to detect the gravitational waves coming from (Newtonian) precessing binaries using the nonprecessing Newtonian template family. In Fig. 8, the probability $P(\mathrm{FF}<\mathrm{FF}_0)$ of getting a FF value below some level FF_0 is depicted. Part (a) of the figure shows this probability for our standard $1.4M_\odot$, $1.4M_\odot$ NS-NS binary for various $\hat{\mathbf{L}}\hat{\mathbf{S}}$ angles. Things look very optimistic in this case; only a very small portion of the geometries produce FF's below 0.9 with a corresponding reduction in the event rate. In Figs. 8(b), by contrast, one can see that for our standard $10M_\odot$, $1.4M_\odot$ BH-NS binary, if the $\hat{\mathbf{L}}\hat{\mathbf{S}}$ angle is large enough ($> 30°$) the FF is below 0.9 for more than half of the various randomly distributed geometries.

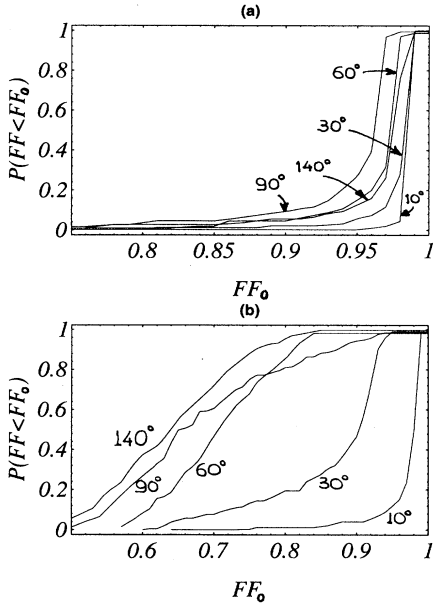

FIG. 8. By compiling the values of the FF for all the cases shown in Fig. 6, we obtain the probability over all the random variables for the FF to stay below some critical value FF_0. The curves in this figure show that probability for various values of the opening angle $\hat{\mathbf{L}}\mathbf{S}$. Plot (a) is for NS-NS binaries and (b) for BH-NS binaries with the same masses and spins as in Fig. 7.

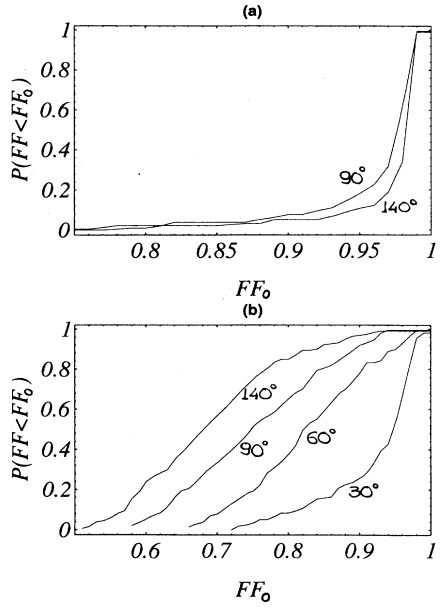

FIG. 9. The same kind of plots as in Fig. 8 but for the (unmodulated) post^1-Newtonian family of templates used to search for modulated Newtonian signals. Again (a) is for NS-NS and (b) for BH-NS. Only a few (the worst) cases are shown here, for comparison with the ones in Figs. 8.

VI. POST-NEWTONIAN TEMPLATE FAMILY

Of course an obvious way to improve the detectability is to use the full family of modulated theoretical waveforms in the search for signals; then, the FF would be unity and we would obtain the maximum possible signal to noise. But this solution is rather undesirable since the modulated waveforms are a very large family containing many parameters, and this would greatly increase the computational task and seriously reduce the statistical significance of any discovered signal. What we need is a variation of the Newtonian filter with only one or two extra parameters that can improve the FF values by better matching the complicated phase evolution of the signals.

As we have seen in Sec. III C, the main reason that a Newtonian template cannot follow the evolution of the PM is that the only frequency evolution of its phase $\Psi(f)$ is $(3/4)(8\pi\mathcal{M}f)^{-5/3}$ [cf. Eq. (26b)], while $\alpha(f)$ [the precession angle; see Eq. (29)] evolves $\propto f^{-2/3}$ or f^{-1} depending on the relative sizes of L and S. A simple way, then, to solve our problem is to add an extra term onto the phase evolution of the Newtonian template, a term with a softer than $f^{-5/3}$ dependence on f, for example an $A f^{-1}$ term, where A is the new template parameter:

$$\tilde{T}_{\mathrm{PN}}(f) = \mathrm{const} \times f^{-7/6} e^{i\Psi_{\mathrm{PN}}(f)}, \tag{35a}$$

with

$$\Psi_{\mathrm{PN}}(f) = 2\pi f t_C - \phi_C + \frac{3}{4}(8\pi\mathcal{M}f)^{-5/3} + A f^{-1}. \tag{35b}$$

Since this $A f^{-1}$ term is also exactly the correction to the phase that is required to match the binary's nonmodulated post^1-Newtonian effects in the waveform [12], this template family (henceforth, we shall call it the "post^1-Newtonian template family") might well be the best one can construct with four parameters $(t_C, \phi_C, \mathcal{M}, A)$ altogether. Our code is able to handle the new parameter in the maximization process to compute the FF. We have attempted a few runs with the extra term for the worst cases we presented in the previous section. It turns out (see Fig. 9) that this extra term helps a lot in matching the modulated Newtonian waveforms, but it still leaves the FF below 0.9 for most of the geometries of our standard BH-NS binary when $\hat{\mathbf{L}}\mathbf{S}$ is greater than $\sim 45°$.

VII. NONMODULATIONAL POST-NEWTONIAN EFFECTS AND A POST$^{1.5}$-NEWTONIAN FAMILY

Up to this point we have assumed modulated Newtonian waveforms as signals. But what about the nonmodulational post-Newtonian effects? We neglected them so as to explore the influence of precession-induced modulation on the FF in isolation from other post-Newtonian effects. Now we are ready to consider these other effects.

As we said in the Introduction, Kokotas, Kròlak, and Schäfer [7] and Balasubramanian, and Dhurandhar [8] have investigated the importance of all the higher nonmodulational post-Newtonian corrections currently available, namely, the post^1- and post$^{1.5}$-Newtonian corrections in the signal, and have found that the Newtonian template family produces rather low FF values for such signals. We have repeated their calculations and confirmed their results. In addition, we have calculated the FF values for all the possible combinations between Newtonian and post-Newtonian nonmodulated signals and templates, and have incorporated the effects of spins, with $\hat{\mathbf{L}}\hat{\mathbf{S}}=0$ (and thus no precession), into the calculations. Of course, when we use signals and templates of the same post-Newtonian accuracy, we get FF values equal to 1.

Before we present our general results, let us write down the form of the most accurate nonmodulated waveform currently available (see Refs. [12,13]), with all the post-Newtonian effects in the amplitude ignored:

$$\tilde{h}_{\mathrm{P1.5N}}(f) = \mathrm{const} \times f^{-7/6} e^{i\Psi_{\mathrm{P1.5N}}(f)}, \tag{36a}$$

where

$$\Psi_{\mathrm{P1.5N}}(f) = 2\pi f t_C - \phi_C + \frac{3}{128}(\pi \mathcal{M} f)^{-5/3}\left[1 + \frac{20}{9}\left(\frac{743}{336}+\frac{11\mu}{4M}\right)x - (16\pi - 4\beta)\,x^{3/2}\right] \tag{36b}$$

and

$$x \equiv (\pi M f)^{2/3}\,, \tag{36c}$$

$$\beta \equiv M^{-2}\hat{\mathbf{L}}\cdot\left[\left(\frac{113}{12}+\frac{25M_2}{4M_1}\right)\mathbf{S}_1 + \left(\frac{113}{12}+\frac{25M_1}{4M_2}\right)\mathbf{S}_2\right]. \tag{36d}$$

One can easily identify the $O(x)$ post^1-Newtonian correction in (36c) as the $A f^{-1}$ post^1-Newtonian term that we introduced in the previous section as an improvement to the Newtonian family.

Table I shows the results of our calculations. Here, by contrast with Secs. IV and V, the signal in each column is unique. The many signal parameters that we faced in Secs. IV and V ($\hat{\mathbf{L}}\hat{\mathbf{S}}$, detector orientation, direction of $\hat{\mathbf{J}}$, direction to source) vanish from the signal in this section's nonprecessing limit, $\hat{\mathbf{L}}\hat{\mathbf{S}}$=0. From Table I, one can see that the FF values for the post$^{3/2}$-Newtonian signal (without precession) and the Newtonian or the post^1-Newtonian template family are much too low for these families to be adequate for detection. These low FF's can be explained by the fact that the signal term $x^{3/2}$ (which is left out of the templates) is comparable with the x term (which the post^1-Newtonian templates include), and has the opposite sign.

Because the Newtonian and post^1-Newtonian families are so inadequate, it is necessary to include higher-order, nonmodulational effects in the waveforms. This can (and should) be done up to the highest available post-Newtonian order, without introducing any new parameters, in the case of vanishing spins. However the waveforms are not yet known beyond post$^{1.5}$-Newtonian order; so for now we only go that high.

More specifically, we introduce a post$^{1.5}$-Newtonian template family whose form is that of Eqs. (36a)–(36d) but with the new spin parameter β set to zero:

TABLE I. We present here the FF values for a Newtonian, a post^1-Newtonian, and a post$^{1.5}$-Newtonian signal with maximal spin [maximal β; where β is given in Eq. (36d)] but no precession, being searched for by three families of templates: the Newtonian family [Eq. (9)], the post^1-Newtonian family [Eq. (35a)], and the post$^{1.5}$-Newtonian family [Eq. (37a)]. Note that the post$^{1.5}$-Newtonian templates are assumed to have $\beta = 0$ in order to keep the number of parameters low. The post$^{1.5}$-Newtonian signals though are chosen to have the maximum possible β parameter by aligning the big object's maximal spin with the angular momentum of the binary (the small object is assumed to have no spin). For every case, two FF values are given, corresponding to a $10M_\odot - 1.4M_\odot$ BH-NS binary and a $1.4M_\odot - 1.4M_\odot$ NS-NS binary. Since modulational effects are absent (the spin and angular momenta are aligned), the binary's orientation does not affect the FF values. The numbers quoted in this table are discussed more extensively in Sec. VII.

	N signal	P^1-N signal	P$^{1.5}$-N signal (β maximal)
N template	1.000 (BH-NS)	0.559 (BH-NS)	0.692 (BH-NS)
	1.000 (NS-NS)	0.465 (NS-NS)	0.594 (NS-NS)
P^1-N template		1.000 (BH-NS)	0.699 (BH-NS)
		1.000 (NS-NS)	0.546 (NS-NS)
P$^{1.5}$-N template ($\beta = 0$)			0.987 (BH-NS)
			0.985 (NS-NS)

$$\tilde{T}_{\mathrm{P1.5N}}(f) = \text{const} \times f^{-7/6} e^{i\Psi'_{\mathrm{P1.5N}}(f)}, \tag{37a}$$

where

$$\Psi'_{\mathrm{P1.5N}}(f) = 2\pi f t_C - \phi_C + \frac{3}{128}(\pi \mathcal{M} f)^{-5/3} \times \left[1 + \frac{20}{9}\left(\frac{743}{336} + \frac{11\mu}{4M}\right)x - 16\pi x^{3/2}\right] . \tag{37b}$$

Again we ignore all the post-Newtonian effects in the amplitude. Note that the $O(x)$ correction is equivalent to the $A f^{-1}$ term of the post^1-Newtonian template.

We have explored the adequacy of this four-parameter $(t_C, \phi_C, \mathcal{M}, A)$ family in searches for waves from nonprecessing but maximally spinning ($\hat{\mathbf{L}}\mathbf{S}$=0) post$^{1.5}$-Newtonian binaries. The resulting FF (0.987 for BH-NS, 0.985 for NS-NS; see Table I) is excellent. The unimportance of the spin effects (the β factor in the signal) is due to the small value of β compared to 4π [see Eq. (36a)]. The situation becomes worse (lower FF) for an extreme ratio of masses (FF $\simeq$ 0.895 for $M_2/M_1 = 0.05$), since for a maximally rotating large black hole (with mass M_1) and a small nonrotating black hole or neutron star (with mass M_2) β grows like the ratio $M_1^2/(M_1+M_2)^2$. (The FF values quoted in Table I for a post$^{1.5}$-Newtonian signal and template assume that only the more massive body is spinning with $\mathbf{S}_i = M_i^2 \hat{\mathbf{L}}$; the more massive was chosen in order to obtain the maximum value for β.)

VIII. MODULATED POST$^{1.5}$-NEWTONIAN SIGNALS SEARCHED FOR WITH THE POST$^{1.5}$-NEWTONIAN FAMILY

We now consider the suitability of this post$^{1.5}$-Newtonian family (37a) for detection of spin-modulated signals. For this purpose we have used as signals the nonmodulated post$^{1.5}$-Newtonian signals for our typical NS-NS and BH-NS binaries and have modulated them according to the AM and PM introduced in Sec. II:

$$\tilde{h}(f) = \mathrm{AM} \times \mathrm{PM} \times \tilde{h}_{\mathrm{P1.5N}}(f) . \tag{38}$$

Although the modulational effects are based on Newtonian orbits and quadrupole wave generation, this artificial composition of signal will surely give us a more realistic kind of signals than just the nonmodulated post-Newtonian or the modulated Newtonian signal.

The FF values we have obtained with our four-parameter post$^{1.5}$-Newtonian templates and the modulated post$^{1.5}$-Newtonian signals were at least as good as the values we obtained in the previous section for unmodulated post^1-Newtonian templates and modulated Newtonian signals; see Fig. 10. This was to be expected since the two terms $x^{3/2}$ and x in the templates' phase [Eq. (37b)] have the exact frequency dependences that the precession follows for the two extreme cases of Eq. (29).

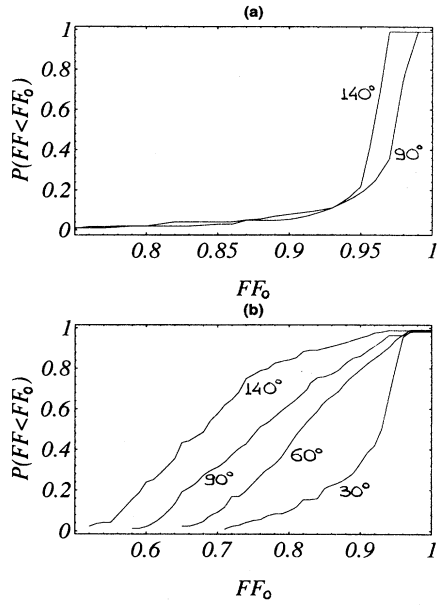

FIG. 10. The same kind of plots as in Fig 9 but for the zero-spin post$^{1.5}$-Newtonian family of Eq. (37a), and a signal in which the Newtonian-order precession effects are added on top of the more realistic post$^{1.5}$-Newtonian signal. Again (a) is for NS-NS and (b) for BH-NS. Only a few (the worst) cases are shown here, for comparison with the ones in Figs. 8.

IX. CONCLUSIONS

This paper is an initial exploratory work on the issue of search templates which will be used by the ground-based LIGO-VIRGO-GEO and space-based LISA detectors, for detecting gravity wave signals from inspiraling black hole and/or neutron star binaries. We have introduced a measure of adequateness of a template family (the fitting factor) and have shown (in agreement with other people's work) that the Newtonian and the post^1-Newtonian template family are inadequate to detect nonmodulated post$^{1.5}$-Newtonian signals. We have then suggested the use of the post$^{1.5}$-Newtonian family with one more parameter than the Newtonian family. The post$^{1.5}$-Newtonian family produces higher FF's than the Newtonian family not only for nonmodulated post$^{1.5}$-Newtonian signals but for precessionally modulated signals too.

The understanding of FF's gained from our study suggests that for most binaries, but not all, an adequate family of search templates will be the four-parameter family (ϕ_C, t_C, $\mathcal{M}$, A), or equivalently (ϕ_C, t_C, $\mathcal{M}$, μ/M), based on the waveforms for circular-orbit, zero-spin binaries at the highest post-Newtonian order $n_{\max}$ that is available when the searches begin. This is likely to be post^3-Newtonian order, i.e., $n_{\max} = 3$. It may well be, however, that as at present ($n_{\max} = 1.5$), and so also then, binaries with moderately large mass ratios and moderately large $\hat{\mathbf{L}}\mathbf{S}$, i.e., with large precessions, will have unacceptably low FF's when this four-parameter family is used. In preparation for that possibility, an

effort is needed now to expand the $n_{\max} = 1.5$, four-parameter family to include some form of modulation that raises the FF above 0.9 in these large-precession cases. This also might be done for the extreme mass-ratio $\mu/M \ll 1$, $n_{\max} = 8$, four-parameter template family based on the Teukolsky-formalism waveforms of Sasaki and Tagoshi [14].

Throughout this paper we have restricted ourselves to template families with continuously varying parameters. Now is the time to abandon that restriction and focus on discrete template families. The goal must be building on the continuous-family insights of this paper and on Refs. [7,8] to devise a discrete family with as small a number of members as possible, which gives FF > 0.9 (or some other threshold) for all plausible binary waveforms. A first exploration of discrete template families has been carried out by Dhurhandhar and Sathyaprakash [6].

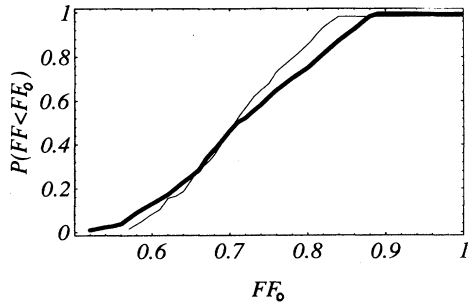

FIG. 11. The same kind of plot as in Fig. 8 but for a $10^6 M_\odot$, $1.4 \times 10^5 M_\odot$ BH-BH binary, with $\hat{\mathbf{L}}\mathbf{S} = 60^0$ and a noise spectrum given by Eq. (A1) (thick line). The corresponding plot for a $10 M_\odot$, $1.4 M_\odot$ BH-NS binary, with $\hat{\mathbf{L}}\mathbf{S} = 60^0$ and a noise spectrum given by Eq. (21) is copied here from Fig. 8 for comparison (thin line).

ACKNOWLEDGMENTS

I am grateful to Kip Thorne for suggesting this problem, and for many helpful discussions and comments. I would also like to thank Éanna Flanagan for many helpful discussions with respect to signal analysis and Eric Poisson for pointing out that the extra term A/f introduced to improve the Newtonian filter is the same as the post^1-Newtonian nonmodulational correction to the waveform. This work was supported in part by NSF Grant No. PHY-92135082 and (in view of its auxiliary implications for space-based gravitational-wave detectors) by NASA Grant No. NAGN-2897.

APPENDIX: EXTENSION OF THE RESULTS TO LOW-FREQUENCY SPACE-BASED DETECTORS

Preliminary designs for a space-based antenna (LISA) to detect gravitational waves from supermassive black holes have been developed, and LISA has been proposed for a future space mission (see Refs. [16]). The noise spectrum for such a detector has been estimated to have roughly the following shape; this is an analytic fit to Fig. 2 of Ref. [15]:

$$S_n(f) = S_0 \times \begin{cases} (f/1\ \mathrm{mHz})^{-4} & \text{for } f < 1\ \mathrm{mHz}, \\ 1 & \text{for } 1\ \mathrm{mHz} < f < 0.1\ \mathrm{Hz}, \\ 10^{-4}(f/1\ \mathrm{mHz})^2 & \text{for } f > 0.1\ \mathrm{Hz}, \end{cases} \tag{A1}$$

with $S_0 = 10^{-42}\ \mathrm{Hz}^{-1}$. Actually, there is one more branch of the noise spectrum for frequencies below 10^{-5} Hz, which grows with decreasing f even faster than $\propto f^{-4}$, but since the noise levels are already so high at these low frequencies, we can ignore this branch and restrict ourselves to the above approximation when computing the FF for binary signals.

There is a great similarity between the shapes of the noise spectra of the ground-based [Eq. (21)] and the space-based [Eq. (A1)] detectors. There is a big difference, however, in the range of frequencies over which these detectors have high sensitivity: five orders of magnitude. The equations describing the precession of a binary and its waveforms depend only on the ratio of masses and the product fM [see Eqs. (2), (3a), (34)]. Therefore, if we use as examples binaries with masses 10^5 times larger than for the binaries considered for the ground-based detectors, and keep the same mass ratios, we should get approximately the same FF values as for the LIGO-VIRGO-GEO detectors. The only differences will come from the modest differences in the shapes of the noise spectra (21) and (A1), and since the spectra are so similar, the FF's should be nearly the same.

We verify this in Fig. 11 for the case of a Newtonian template family and a maximally rotating $10^6 M_\odot$ and a nonrotating $1.4 \times 10^5 M_\odot$ BH-BH binary, with $\hat{\mathbf{L}}\mathbf{S} = 60°$ and a noise spectrum given by Eq. (A1). The corresponding plot of the FF probability distribution over the random variables for a $10 M_\odot$, $1.4 M_\odot$ BH-NS binary, with $\hat{\mathbf{L}}\mathbf{S} = 60°$ and a noise spectrum given by Eq. (21), is copied here from Fig. 8 for comparison. The fairly good agreement is obvious. Thus, all the results derived in this paper for LIGO-VIRGO-GEO search templates can be carried over essentially without change to LISA, and this paper can be regarded as an initial exploratory study of templates for LISA as well as for LIGO-VIRGO-GEO.

[1] A. Abramovici *et al.*, Science **256**, 325 (1992).
[2] B. F. Schutz, in *The Detection of Gravitational Waves*, edited by D. G. Blair (Cambridge University Press, Cambridge, England, 1991), pp. 406–452.
[3] K. S. Thorne (private communication).
[4] T. A. Apostolatos, D. Kennefick, A. Ori, and E. Poisson, Phys. Rev. D **47**, 5376 (1993).
[5] G. Quinlan and S. L. Shapiro, Astrophys. J. **321**, 199 (1987).
[6] S. V. Dhurhandhar and B. S. Sathyaprakash, Phys. Rev. D **49**, 1707 (1994).
[7] K. Kokkotas, A. Kròlak, and G. Schäfer, in Proceedings of the Moriond 94 Workshop (unpublished).
[8] R. Balasubramanian and S. V. Dhurandhar, Phys. Rev. D **50**, 6080 (1994).
[9] C. M. Will, in *Proceedings of the Eighth Nishinomiya-Yukawa Symposium on Relativistic Cosmology*, edited by M. Sasaki (Universal Academy Press, Tokyo, in press).
[10] C. Cutler and E. Flanagan (in preparation).
[11] T. A. Apostolatos, C. Cutler, G. J. Sussman, and K. S. Thorne, Phys. Rev. D **49**, 6274 (1994).
[12] C. Cutler and E. Flanagan, Phys. Rev. D **49**, 2658 (1994).
[13] A. G. Wiseman, Phys. Rev. D **46**, 1517 (1992).
[14] H. Tagoshi and M. Sasaki, Phys. Rev. D **51**, 1646 (1995).
[15] K. Danzmann, A. Rüdiger, R. Schilling, W. Winkler, J. Hough, G. P. Newton, D. Robertson, N. A. Robertson, H. Ward, P. Bender, J. Faller, D. Hils, R. Stebbins, C. D. Edwards, W. Folkner, M. Vincent, A. Bernard, B. Bertotti, A. Brillet, C. N. Man, M. Cruise, P. Gray, M. Sandford, R. W. P. Drever, V. Kose, M. Kühne, B. F. Schutz, R. Weiss, and H. Welling, "LISA: Proposal for a Laser-Interferometer Gravitational Wave Detector in Space," European Space Agency report, 1993 (unpublished); available as document MPQ 177 from the Max-Planck-Institut für Quantenoptik, 8046 Garching bei München, Germany.

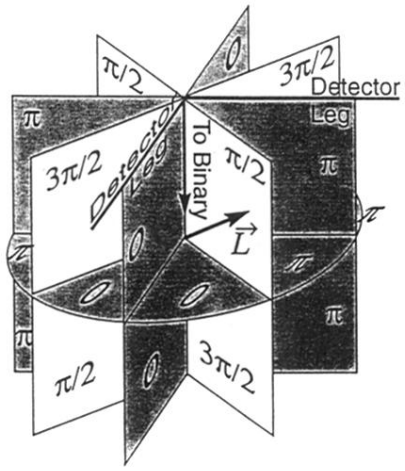

FIG. 5. This *cell diagram*, reproduced from Ref. [11], is a useful tool for understanding how the phase φ evolves while $\hat{\mathbf{L}}$ precesses, for a detector positioned as shown in the diagram. Each wall in the diagram is labeled by the value that φ takes when $\hat{\mathbf{L}}$ lies in that wall. The lines at which black and white walls intersect are singular directions; when $\hat{\mathbf{L}}$ passes near such a line, φ changes rapidly.

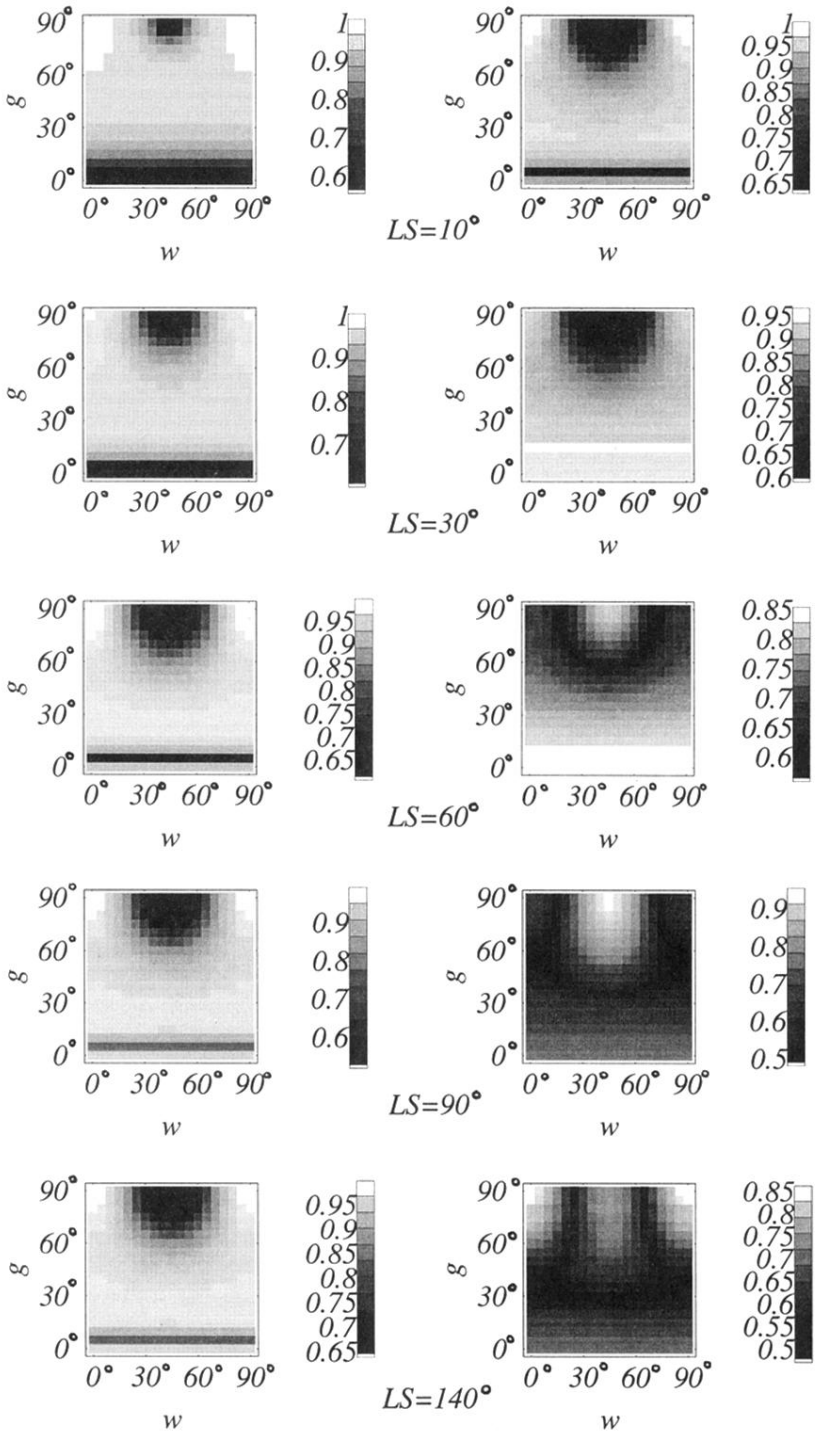

FIG. 6. This is a series of density plot diagrams showing the FF distribution in a grey scale (black represents the lowest values) for a detector at the North Pole as one rotates its arms (variable w) and changes the inclination g of the binary's total angular momentum $\mathbf{J}$ to the z axis (the Earth's rotation axis) while keeping $\mathbf{J}$ in the y-z plane (see Fig. 3). We have arranged the figures in pairs. The left column corresponds to a $1.4M_\odot$, $1.4M_\odot$ NS-NS binary and the right column to a $10M_\odot$, $1.4M_\odot$ BH-NS binary. For both types of binaries the more massive object is maximally spinning ($S_i = M_i^2$). The ring with the low FF around the singular direction ($g = 90°$, $w = 45°$) can be easily recognized. Actually only one-eighth of the whole (g, w) space is displayed here since the same pattern is repeated.